Journal of Materials Chemistry B

Accepted Manuscript

ROYAL SOCIETY OF CHEMISTRY

www.rsc.org/materialsB

Journal Name

ARTICLE

Bimetallic silver nanoparticle-gold nanocluster embedded composite nanoparticles for cancer theranostics

Received 00th January 20xx,
Accepted 00th January 20xx

DOI: 10.1039/x0xx00000x

www.rsc.org/

Deepanjalee Dutta,[a] Amaresh Kumar Sahoo,[b] Arun Chattopadhyay [a,c]* and Siddhartha Sankar Ghosh [a,b]*

A bimetallic silver nanoparticle based gold nanocluster module has been developed for theranostic cellular application by a rapid and simple galvanic exchange method. The use of chitosan as a template has helped to convert the bimetallic system into the composite nanoparticles, which can be easily delivered into cancer cells. The synthesized composite nanoparticles offer the advantage of combinatorial properties of the metals present in two different nanoscale levels enabling both killing and bioimaging of cancer cells. The detailed molecular events of cell death was illustrated for this combined module to decipher apoptotic mediated cell death.

Introduction

Possibilities to create nanoscale materials with desired properties have been in focus to address several issues in the field of cancer medicine.[1,2] The ultimate target of these nanomaterial based techniques is to diagnose cancer at nascent stages and to fabricate effective anti-cancer agents targeting signalling pathway for effective drug delivery or gene silencing. Presently efforts in nanomedicine are to embed both therapy and diagnosis in a single entity i.e., ‘nanotheranostics’.[3, 4] By exploring size dependent physicochemical properties, the noble metal nanoparticles had emerged as promising materials for therapy as well as diagnosis. Silver nanoparticles (Ag NPs) are known to induce apoptosis by ROS generation and subsequent DNA damage.[5] Also nanoparticles conjugated to different organic dyes have been in use for cancer imaging and diagnostic applications.[6,7,8] However these organic dyes suffer from several disadvantages like narrow stokes shift, photoblinking, low stability, shorter lifetime.[9] Further, decreases in the length scale of the metal NPs, in the range of < 2 nm, led to ultra-small nanoparticles known as nanoclusters, which are fascinating in the field of nanophotonics. Numerous methods have been developed for the synthesis of these metal clusters using proteins, DNA, polymers as templates in presence of thiols, some requiring the use of additional reducing agents, further functionalization have been achieved by using capping agents.[10,11,12] These metal clusters owe some extraordinary properties like inherent luminescence attributing to their small size, enhanced photo stability, longer lifetime, large stokes shift, lower toxicity, making them excellent candidates to be used as imaging agents, catalysts in biological applications.[13,14] For instance AuNCs have been used for bioimaging due to its excellent stability, biocompatibility, emission in red region allowing differentiation of cellular autofluorescence. Further, to maximise the use of metal NCs as *in vitro* as well as *in vivo* probes special characteristics such as specificity, cell penetration ability, intracellular environment monitoring, toxicity, clearance have been explored.[15-19] Hence, a conjugation of nanoclusters with nanoparticles would be an ideal candidate for developing an efficient and advanced smart theranostic vehicle.

Bimetallic systems are preferred rather than single metal system as it gives an opportunity to combine the properties of two metals in a single entity making it a smartly architected nanostructure.[20] There are various methods reported by which bimetallic nanoparticles, nanoclusters can be synthesized. It can be broadly classified into co-reduction methods involving addition of both metal ions salt precursors followed by reduction and post treatment methods like core etching, galvanic replacement etc.[21,22] Also synthesis of bimetallic hollow NPs have also been reported by galvanic replacement method.[23] Silver and gold are one of the most widely used bimetallic systems due to the ease in synthesis.[24] The so far studied bimetallic nanocluster systems focused mainly on enhanced luminescence intensity, catalytic property of bimetallic systems over monoatomic ones.[25-27] However, less reports are available on evaluation of therapeutic potential of bimetallic nanocluster systems. Recently the effect of luminescent Au NCs on various cancer cell lines have been studied alongside bioimaging.[28] Also another work which

---

[a] Centre for Nanotechnology, Indian Institute of Technology Guwahati, Guwahati –781039, India.
[b] Department of Biosciences and Bioengineering, Indian Institute of Technology Guwahati, Guwahati –781039, India
[c] Department of Chemistry, Indian Institute of Technology Guwahati, Guwahati –781039.

† Footnotes relating to the title and/or authors should appear here.
Electronic Supplementary Information (ESI) available: [details of any supplementary information available should be included here]. See DOI: 10.1039/x0xx00000x

employed bimetallic AgAuNCs for cellular applications reported non-cytotoxicity towards cancer cells except at a very high silver concentration.[29] Hence, it is anticipated that a combined system including both Ag NPs and luminescent Au NCs would serve the purpose of anticancer activity and bioimaging better than monoatomic system. Also the importance of biocompatible composite nanoparticles as carriers for effective and sustained delivery of these metal NPs into cancer cells is a demand of the situation. The potential of nanocarriers based on dendrimers, liposomes, hydrogel, polymeric NPs in drug delivery have been well established but the use of these in delivery of metal NPs is less explored.[30,31] Keeping all these elements in mind, herein we report an easy aqueous synthesis of the AuNCs [standard reduction potential of $AuCl_4^- + 3\ e^- = Au(0) + 4\ Cl^-$ is $1.00E^o$ (V)] by Galvanic replacement of AgNPs [standard reduction potential of $Ag^+ + e^- = Ag(0)$ is $0.80E^o$(V)] with biocompatible chitosan polymer as a template harbouring both the AgNPs and AuNCs, which was further converted into a theranostic composite nanoparticles(AgNP-AuNC-CSNPs) by crosslinking of the polymer using sodium tripolyphosphate[32] which acted as a carrier to deliver the AgNPs and AuNCs inside cancer cells. The synthesis procedure involves initial preparation of AgNPs on chitosan by reduction in basic condition. Then AuNCs were prepared alongside AgNPs by treating with mercaptopropionic acid (MPA). Generally, the formation of bimetallic nanoclusters or coreshell nanoparticles takes longer time, harsh reaction conditions, and extensive purification steps. The present method of water soluble bimetallic nanoparticle-nanoclusters synthesis can be marked as a simple and rapid method. The effect of these theranostic composite nanoparticles was studied in human cervical cancer cell line (HeLa). The disadvantages of using chitosan along with gold nanoclusters is the poor solubility of native chitosan at pH above 6.5 which is generally resolved by the use of modified chitosan[33, 34] and the excitation of gold nanoclusters which is in the UV region making it difficult to be used in *in vivo* applications[35], although there are reports of use of UV excitation dependent materials in *in vivo* biomaging applications also.[36, 37] Furthermore considering the numerous advantages like low toxicity, high photo stability, water solubility, ultrasmall size enabling deeper tissue penetration of gold nanoclusters compared to quantum dots and organic dyes as biological probes and use of a natural polymer chitosan as a stabilizer makes the system more biocompatible, biodegradable rather than those involving use of organic moieties[38], with enhanced permeation and mucoadhesive properties suitable for systemic nanocarrier based applications. In addition, the possibility of using gold nanoclusters for two photon imaging *in vitro*, with both excitation and emission wavelengths in the NIR region, has been demonstrated.[17] This also makes the use of gold nanoclusters appealing. On a promising note, a reduction of cell viability was observed in the bimetallic system, and a comparative study was done with AgNPs only. Along with cytotoxic nature, the system facilitated bio-imaging of the cancer cells. The detailed mechanism of cell death established apoptosis mediated cell death. Thus, these theranostic composite nanoparticles killed cancer cells and provided option for concomitant cellular imaging.

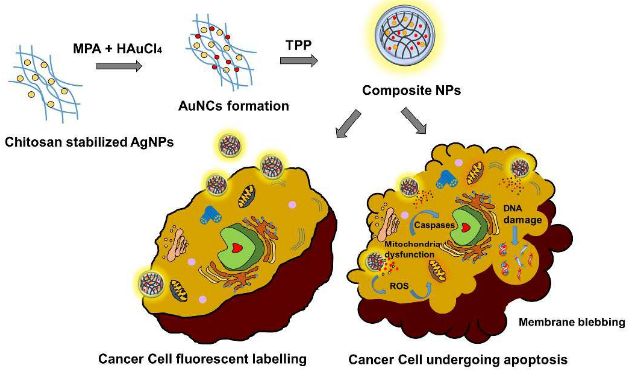

Scheme 1: The scheme illustrates synthesis and delivery of bimetallic composite nanoparticles for bioimaging and induction of apoptosis in cancer cells.

Experimental Section

Materials and Methods

Chemicals: For the synthesis mentioned below, $HAuCl_4$ (Au, 17 wt% in dilute HCl; 99.99%, Sigma Aldrich), $AgNO_3$(Merck), chitosan (Mw 672 KDa, Sigma Aldrich), sodium hydroxide (Merck), mercapto propionic acid (Sigma Aldrich), sodium tripolyphosphate (TPP, Sigma Aldrich), Milli-Q grade water (> 18 MΩ cm^{-1}, Millipore) were used without any alterations.

Synthesis of AgNP-AuNCs: For the synthesis of luminescent AgNP-AuNCs, 0.5% (w/v) chitosan solution was initially prepared by dissolving 500 mg/ 100mL in Milli Q water containing 0.1% (v/v) acetic acid. After filtering out the undissolved residues, pH of the resultant solution was adjusted to 6.4 using 5M NaOH. Then, a solution was prepared by successive addition of 10 mL of Milli Q water, 1 mL of the filtered chitosan, 400 µL of 10 mM $AgNO_3$ and then heated to 90 ^{0}C. As soon as it started to boil, 400 µL of 0.3 M NaOH was added drop wise. The colour of the solution turned light brown which indicated the formation of silver nanoparticles.[39] The reaction was allowed to proceed for 10 min and then cooled to room temperature. The hence formed AgNPs were centrifuged (10000 rpm, 10 min) and the supernatant was discarded. The pellet containing AgNPs was redispersed in 10 mL water with pH adjusted to 6.4. Then 2 mL of these AgNPs solution was taken and subsequently 1 mL of water, 8 µL of 0.11 M mercapto propionic acid (MPA, Sigma Aldrich) and 20 µL of 10 mM $HAuCl_4$ were added and the mixture was stirred for 5 min. The final solution contained both AuNCs and AgNPs and were characterized for confirmation.

Synthesis of AgNP-AuNC chitosan composite nanoparticles: Chitosan nanoparticle synthesis was done by a slightly modified method from that developed by Calvo et al,.[40] With the rest of the traditional method followed, herein, 0.2 mg/mL sodium tripolyphosphate (TPP, Sigma Aldrich) was added drop-wise to 3mL solution of above synthesized AgNP-AuNCs under constant stirring condition at room temperature to prepare chitosan composite nanoparticles. AgNP-chitosan NPs (without AuNCs) were synthesized by the same method, keeping concentration of chitosan and $AgNO_3$ constant.

Characterization Studies

UV visible spectroscopy: The absorbance characteristics in UV-Vis region of the as synthesized AgNPs, AgNP-AuNCs were examined with UV-visible spectrophotometer JASCO V-630.

Transmission electron microscopy (TEM): The sample preparation for the TEM analysis was done by diluting 500 µL of the composite solution in 500 µL water and out of which 7 µL was drop-cast onto the TEM grids. The dried TEM grid was examined under transmission electron microscope (TEM; JEM 2100; Jeol, Peabody, MA, USA), operating at a maximum accelerating voltage of 200 keV.

Luminescence Measurements: All luminescence measurements were performed using fluorescence spectrophotometer LS55, Perkin Elmer and Horiba Flurolog3.

Quantum yield measurements:

For quantum yield (QY) measurements of the AgNP-AuNCs a conventional method was followed by using quinine sulfate in 0.10 M H_2SO_4 solution as standard. The calculation of the absolute value of QY was done on the basis of the following equation

$$QY = QY_r \frac{m}{m_r} \frac{n^2}{n_r^2}$$

Here, m is the slope of integrated luminescence intensity vs. absorbance plot, n is the refractive index and suffix r refers to reference quinine sulphate solution. The absorbance and the luminescence intensity was measured simultaneously using the same solution. The refractive index of solvent (water) is 1.33, quantum yield of the standard (QYr) is 0.54

Dynamic Light scattering study: For the measurement of hydrodynamic diameter and the zeta potential, AgNP-AuNCs (composite NPs) was assessed using Malvern Zetasizer Nano ZS.

Matrix-assisted laser desorption ionization time-of-flight mass spectrometry (MALDI-TOF MS) analysis: MALDI–TOF (Applied Biosystems 4800 Plus MALDI TOF/TOF Analyzer) analysis was performed using R-cyano-4-hydroxycinnamic acid (CHCA) matrix.

Fourier transform infrared (FTIR) spectroscopy: To carry out FTIR analysis, samples were initially lyophilized and then pellets were prepared after mixing with KBr. The pellets were characterized by Perkin-Elmer Spectrum One machine in the range of 4000 - 400 cm^{-1}.

Atomic absorption spectroscopy (AAS): The amounts of silver and gold present in AgNPs and AgNP-AuNCs (composite NPs) were determined using Atomic absorption spectrophotometer AA240 - Varian Inc.

Cellular Activity Studies

Cell Culture: For cell culture studies, HeLa cells (human cervical carcinoma) were procured from National Center for Cell Sciences (NCCS), Pune, India. These cells were cultured in Dulbecco's Modified Eagle's Medium supplemented with L-glutamine (4 mM), penicillin (50 units/mL), streptomycin (50 mg/mL, Sigma-Aldrich) and 10% (v/v) fetal bovine serum (PAA Laboratories, Austria) in 5% CO_2 humidified incubator at 37 ^{0}C.

Epi-Fluorescence Microscopy: The cells were treated with composite NPs and imaged under an epi-fluorescence microscope (Nikon ECLIPSE, TS100, Tokyo) under UV (340-380nm) excitation. Briefly, the sample preparation for imaging involves incubation of 1× 10^6 HeLa cells (seeded into a cover slip contained in a 35mm culture plate) for 24 h. The hence incubated cells were treated with composite NPs for 6 h. Following which, the medium was discarded and the cells were washed with 1X PBS for visualization under microscope.

Deconvolution Fluorescence Microscopy: The cells were treated with composite NPs and imaged under Delta Vision deconvolution microscope (G E Healthcare). Herein, the sample preparation for imaging involves incubation of 1× 10^6 HeLa cells (seeded into a cover slip contained in a 35mm culture plate) for 24 h. The hence incubated cells were treated with composite NPs for 6 h. The medium was then discarded and the cells were washed with 1X PBS for visualization under microscope.

MTT assay: For cell viability studies, 1×10^5 HeLa cells/well were (seeded in 96-well microtiter plate) grown overnight in 5% CO_2 humidified incubator (37 ^{0}C for 24 h). These cells were subsequently treated with composite NPs. MTT (3-(4, 5-dimethylthiazolyl-2)-2, 5-diphenyltetrazolium bromide) assay was carried after 24 h to obtain the number of viable cells. Mitochondria reduces MTT into color formazan in living cells. Thus, absorbance at 550 nm reveals the amount of formazan product, which is directly proportional to the number of living cells. However, there is a background interference due to absorbance at 690 nm which is to be addressed. The % of cell viability was calculated as

$$\% \textbf{ viable cells} = \frac{(\boldsymbol{A550 - A690})\ \boldsymbol{of}\ (\boldsymbol{NP})\ \boldsymbol{treated\ cells}}{(\boldsymbol{A550 - A690})\boldsymbol{of\ control\ cells}} \times \mathbf{100}$$

Acridine Orange/Ethidium Bromide Staining: Also for AO/EB staining, 1×10^5 HeLa cells/well were (seeded in 96-well microtiter plate) grown overnight in 5% CO_2 humidified incubator (37 ^{0}C for 24 h) and were subsequently treated with composite NPs. The treated cells were stained with AO/EB (Sigma-Aldrich) dual dyes. After removing the culture media, cells were washed twice with PBS and stained by adding 5 µL of 1 mg/mL EtBr and 2 µL of 1 mg/ml AO. The cells were then incubated for 10 min and were washed again with PBS for visualization under fluorescence microscope (Nikon ECLIPSE, TS100, Tokyo) with an excitation filter of 480/30 nm.

Field emission Scanning Electron Microscopy (FESEM): FESEM analysis were carried out to reveal the cell morphology prior and after the treatment with composite NPs. Briefly, the sample preparation involves, growth of cells (1 x10^5 cells/well, 6-well tissue culture plates) and then treatment with composite NPs. These cells were fixed in 0.1% formaldehyde after being washed with PBS. Centrifugation of this cell suspension is done and the pellet is redispersed in PBS. Following this, the cells were drop-cast on aluminium foil covered glass slide and were allowed to dry for analysis.

Uptake studies of composite NPs in HeLa cells by TEM: The uptake of composite NPs by cells was examined under transmission electron microscope. The sample preparation involved initial growth of HeLa (1×10^5 cells, 35 mm culture dishes) cells and then they were treated with composite for 1 h, 3 h, 6 h, 12 h and 24 h. These cells were then harvested by trypsinisation followed by centrifugation (650 rcf, 6 min) and finally were fixed in (or with) 70 % chilled ethanol. For the TEM analysis, 7 uL of this sample was drop-cast onto copper TEM grids.

Determination of Reactive Oxygen Species (ROS): For ROS determination, HeLa cells (1x 10^5 cells/well, seeded in 6-well plate) were grown for 24 h and then treated with composite NPs for 3 h. These cells were incubated for 10 min after adding 1 mM 2,7-dichlorofluoresceindiacetate (5 µL /well, DCFH-DA, Sigma-Aldrich). After discarding the media, the cells were harvested and redispersed in fresh media. DCFH-DA (non-fluorescent dye) can readily diffuse inside the cell where it is converted to DCFH through hydrolysis. Thus, formed DCFH will be ultimately transformed to dichlorofluorescein (DCF, green fluorescent) upon oxidation. Hence, samples were analyzed for DCF fluorescence in FL1-H channel in a flow cytometer (FacsCalibur, BD Biosciences, NJ) at an excitation wavelength of 488 nm and emission wavelength of 530 nm. The fluorescence data were recorded with the Cell Quest program (BD Biosciences) for 15000 cells in each sample.

Cell Cycle Analysis: Propidium iodide staining method was adopted for cell cycle analysis. Initially, HeLa cells (1x 10^5 Cells, 6 well plates) were grown and then were treated with composite NPs for 24 h. Here, for both treated and the control cells, the media and PBS were collected separately. These cells were then harvested by trypsinization. After harvesting, the cells along with the media and collected PBS were centrifuged (650 rcf, 6 min). Following this, the cells were fixed by slowly adding 1 mL of cold 70% ethanol under vortexing and was stored at 4 ^{0}C. The cells were then centrifuged and washed in ice-cold PBS. Upon washing, these cells were treated with RNase for 1 h at 55 ^{0}C. To this, 10 uL of 1 mg/mL PI was added and incubated (37 ^{0}C, 30 min) in the dark. The samples were then analyzed in a FACSCalibur (BD Biosciences, NJ). PI fluorescence data were recorded with the CellQuest program (BD Biosciences) for 15000 cells in each sample and subsequently analyzed.

Caspase 3 assay: Sample preparation for Caspase 3 assay involved growth of HeLa cells (1x 10^5 cells/well, 6 well plates) followed by treatment with composite NPs for 24 h. These treated cells were then harvested by trypsinisation and fixed in 0.1% formaldehyde for 15 min. After fixing, the samples were centrifuged (650 rcf, 6 min) and the pellet was redispersed in PBS. 0.5% of Tween 20 was added to this and was incubated in dark for 20 min. Following this, the cells were washed with PBS thrice and then 10 µL of PE conjugated anticaspase 3 antibody was added. Finally, these cells were incubated for half an hour at 37 ^{0}C and were analysed for PE fluorescence in FACSCalibur (BD Biosciences, NJ).

RT–PCR for caspase expression: Total RNA was extracted from HeLa cells and the cDNA was prepared using Verso cDNA kit (Thermo Scientific). Then, cDNA was amplified by polymerase chain reaction (PCR) using 2X BiomixRed(Bioline) and IDT (Integrated DNA technologies) forward primer 5'-TTTGTTTGTGTGCTTCTGAGCC-3' and the reverse primer 5'-ATTCTGTTGCCACCTTTCGG-3' which is specific for the gene Caspase 3 and Beta actin served as control with forward primer 5'-CTGTCTGGCGGCACCACCAT -3' and reverse primer 5'-GCAACTAAGTCATAGTCCGC -3' . The PCR amplification condition was maintained as, denaturation at 94 ^{o}C for 60 s, annealing at 55 ^{o}C for 60 s and extension at 72 ^{o}C for 60 s.

Results and discussion

AgNP-AuNCs appeared as brown color dispersion with UV- Vis absorbance at 425 nm indicating presence of silver nanoparticle (Figure 1A). In case of control silver nanoparticle, the UV-Vis peak found at 410 nm was slightly red shifted after addition of MPA, which may be attributed to the change in dielectric constant[41] of the stabilizing layer (of the AgNPs) in addition to some aggregation in presence of thiol group containing molecules.[42] The surface plasmon property was still persistent after treating AgNPs with MPA and subsequent formation of AuNCs, unlike in previously reported cases where complete disappearance of plasmonic property was observed.[43,44] In certain cases for gold nanoclusters absorption at around 300-400 nm due to the "d-sp, sp-sp" transitions or formation of thiolate complexes has been reported.[45] Nevertheless, there are reports supporting complete disappearance of UV absorbance after formation of nanoclusters.[46] Here, the galvanic replacement yielded metal nanoclusters, possibly due to the reaction of the as-formed Au-thiolate complexes by reaction of HAuCl4 in the presence of MPA with AgNPs[46] within the biopolymer chitosan, which acted as a template for directed synthesis of metal clusters. Possibly along with Ag NPs, the presence of the thiol (in MPA) as the stabilizing ligand and appropriate amount of template (chitosan) provided protection due to its bulk nature, facilitating the formation of AgNP-AuNCs. Plasmonic absorption peak for Au NPs was missing (as inferred from the absorption spectrum) whereas that for AgNPs was prominent at 425 nm. Thus in the composite, possibly AuNCs and AgNPs were present and larger particles of AuNPs were absent. The time dependent UV-Vis spectra remained unaltered, indicating that stable products were formed (refer to Electronic Supplementary Information, Figure S1A). The same sample upon excitation by UV light (300 nm) exhibited a strong emission peak at 620 nm which indicated formation of AuNCs (Figure 1B) and a comparatively weaker peak in the region of 400-500 nm possibly due to chitosan[47](refer to Electronic Supplementary Information, Figure S1B). The luminescence intensity of AgNP-AuNCs could be tuned when synthesized in different ratios of the precursors. Keeping the concentration of $AgNO_3$ constant, with increasing concentrations of $HAuCl_4$ a gradual increase in luminescence intensity was observed alongside loss of SPR peak due to etching of silver nanoparticles by gold salts (refer to Electronic Supplementary Information, Figure S1C,D). But, when the reverse process was performed, that is, with increasing concentration of silver, keeping gold concentration constant an interesting observation was made. The luminescence of gold clusters was optimised with increasing of silver content, and a luminescence enhancement(red) effect was seen at higher silver concentrations[48,49,50](refer to Electronic Supplementary Information, Figure S2A). However, for the cellular studies, optimum concentrations of Au and Ag were standardized where both the SPR peak of AgNPs and luminescence of AuNCs prevailed.

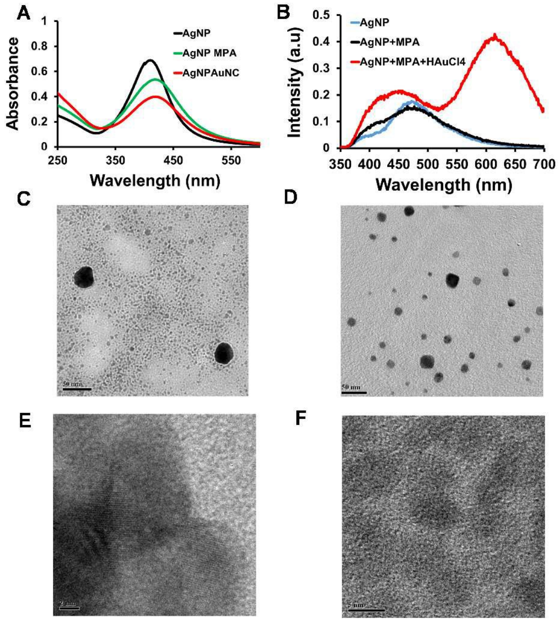

Figure 1. (A) The UV-Vis absorption spectra of the Ag NPs, AgNPs after reacting with MPA and AgNP-AuNCs. (B) Emission spectra of the AgNP-AuNCs showing the emission peak at 620 nm when excited at 300 nm. (C) TEM images of the AgNP-AuNCs at 50nm scale bar. (D) TEM images of initial Ag NPs at 50 nm scale bar. (E) HRTEM images of Ag NPs and (F) Au NCs present in AgNP-AuNCs.

TEM investigation showed formation of AgNP-AuNCs when compared to initial AgNPs (Figure 1C and1D). The HRTEM image for bigger particles which are likely to be Ag nanoparticles (as inferred from the absorption spectrum of Figure 1A) showed lattice spacing of 0.22 nm which corresponds to Ag. However, HRTEM image of small size particles possibly due to Au NCs did not show any distinct lattice spacing (Figure 1E and1F).The SAED pattern corresponded to AgNPs, but didn't show any distinctive signature for AuNCs (refer to Electronic Supplementary Information, Figure S3A). The EDX spectrum of the particles confirmed presence of both Ag and Au (refer to Electronic Supplementary Information, Figure S3B) which was supported by the HAADF-STEM(BF) image of AgNP-AuNCs and corresponding EDX mapping of Ag and Au (refer to Electronic Supplementary Information, Figure S4A,B,C). The average diameter of the particles revealed two different size distributions of 1.41$\underline{+}$ 0.41nm corresponding to AuNCs and the size distribution of AgNPs showing majority of the particles in 3-10nm range along with few particles of bigger size (refer to Electronic Supplementary Information, Figure S5). Also MALDI-TOF analysis of the sample (refer to Electronic Supplementary Information, Figure S6) showed a peak at 5390, which was justified by formation of $[Au_{20}\,(MPA)_{13} + 4Na^{+} - 4H^{+}]^{4-}$; hence we may conclude that there are 20 Au atoms in the metal cluster core. The presence of additional peaks could be due to fragmentation of the sample or formation of other NCs in small numbers. The photostability studies of emission intensity of the NCs revealed that the NCs were stable compared to standard rhodamine 6G. The fluorescence intensity decrease rate (F/F_0) of the NCs was 0.0025 % per sec, whereas in case of commonly used fluorescent dye such as, rhodamine 6G, the rate was found to be 0.095 % per sec. The quantum yield of the AgNP-AuNCs was measured to be 2.3% using quinine sulfate as standard (refer to Electronic Supplementary Information, Figure S7A and S7B) and was deemed suitable for imaging applications.[51] The FTIR spectra of the AgNPs when compared to control chitosan showed prominent shift in the peak of –NH bending from 1609 cm^{-1} to 1570 cm^{-1}, suggesting interaction of the as formed AgNPs with –NH group of chitosan. Also the –SH stretching of MPA, which occurred at 2580 cm^{-1} for free MPA disappeared after formation of AuNCs, possibly due to –S-Au bond formation.[52,53] (refer to Electronic Supplementary Information, Figure S8A –S8D).

An important application of this bimetallic system with dual nature of SPR and luminescence is as a theranostic agent. The luminescence of AuNCs can be used for imaging and further cytotoxicity is provided by the presence of AgNPs. With the help of ionic gelation method, chitosan biopolymer composite can easily be converted into nanoparticles with its intact luminescent property of the NCs for delivery into cancer cells as a smart theranostic vehicle (Figure 2A and 2B).The luminescence enhancement observed after addition of TPP is probably due to aggregation of nanoclusters. Similar observation has been made in the presence of Zn^{2+} ions.[54] during chitosan nanoparticle formation. The mean hydrodynamic diameter of the hence prepared composite NPs (AgNP-AuNC-CSNPs) was 155.5 nm, with having zeta potential +19.3mV, which are generally considered favourable for cellular delivery applications.[55] (Refer to Electronic Supplementary Information, Figure S9A and S9B).

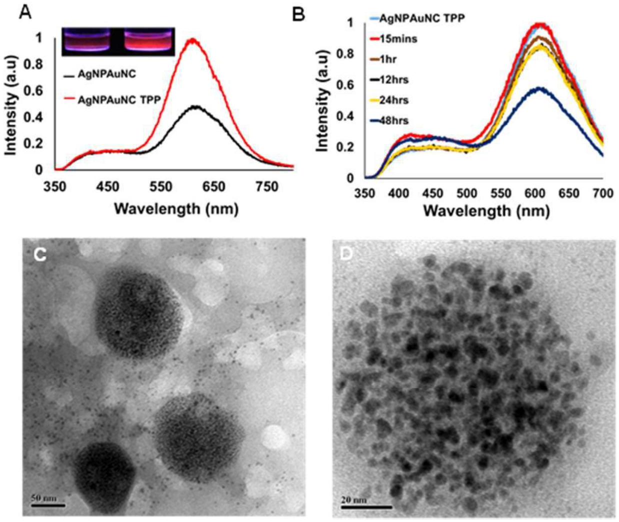

Figure 2. (A) Luminescence spectra of the AgNP-AuNCs before and after addition of TPP (inset contains images of AgNP-AuNC before and after addition of TPP under UV transillumination). (B) Time dependent emission spectra of composite NPs. (C) TEM image of the composite NPs. (D) Magnified TEM image composite NP.

Additionally, TEM images revealed that the average size of the composite NPs was 120 ± 20 nm (Figure 2C and 2D) and FESEM images too exhibited the size to be 120 ± 30 nm (Refer to Electronic Supplementary Information, Figure S9C). Further, the presence of both gold and silver was confirmed by atomic absorption spectroscopy (AAS). The presence of unreacted ions was eliminated by repeated washing of the sample after centrifugation. The concentrations of Ag and Au in the as-synthesized composite used were found to be 0.68 μg/mL and 0.0017μg/mL, respectively. Thereby, an easy rapid fabrication of smart bimetallic theranostic vehicle was achieved with the conjugation of gold nanoclusters and silver nanoparticles.

To analyse the capability of these bimetallic chitosan composite NPs for possible use as intracellular probes, human cervical cancer (HeLa) cells were incubated with 80 μg/mL of the NPs in cell culture medium for 3 h and then the cells were imaged under fluorescence microscope. The control cells showed no fluorescence (Figure 3A-3C) and the presence of the fluorescent nanoclusters was seen inside the treated cells as shown in (Figure 3D-3F), which was supported by a high resolution deconvolution fluorescence microscopy image (Figure 3H-3J). Here, it is to mention that these composite NPs (AgNPs-AuNC embedded) should be non-cytotoxic for fluorescent probing. Hence, a lower concentration (80 μg/ml) than toxic dose for short duration was applied for imaging applications. The uptake of composite NPs was evident from the TEM analysis. The incorporation of the composite (Ag NPs with Au NCs) inside the cell was clearly observed, and the extensions of the plasma membrane suggests possible endocytosis mediated uptake of the composite NPs[56] (Figure 3K and 3L). The average size of the composite NPs was similar to the as-synthesized ones, confirming overall stability of the particles after uptake, which is essential for optimal activity. The time dependent TEM analysis provides an idea of how the cell progresses towards apoptosis by visualizing the changes in the plasma membrane at different time points (refer to Electronic Supplementary Information, Figure S10A-S10E). In addition to the conventional methods, this approach provides a new insight to monitor uptake of the composite NPs by cancer cells where alteration of cell membrane was also seen in TEM images.

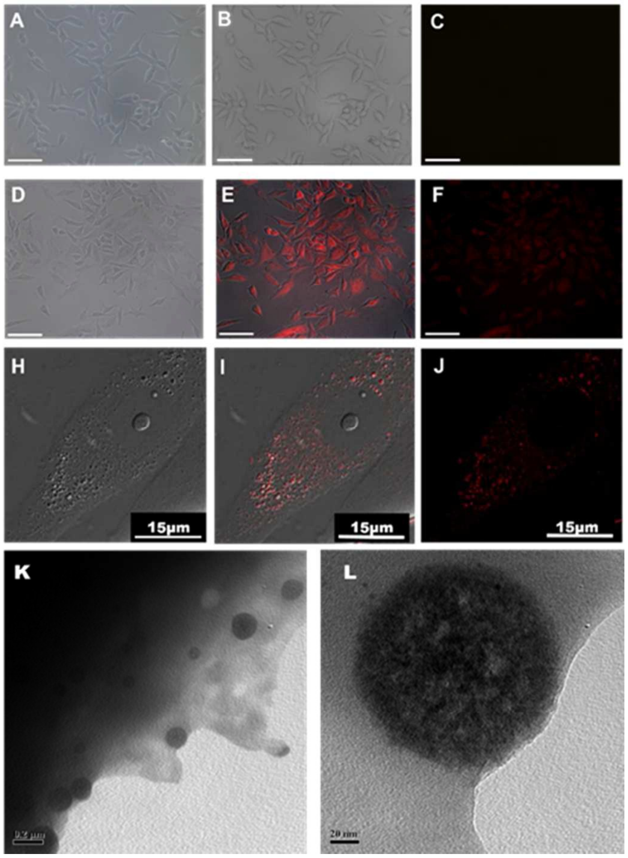

Figure 3. Epi fluorescence microscopic images of control HeLa cells ; (A) bright field image; (B) the merged fluorescent image. (C) Fluorescence image and HeLa cells treated with composite NPs for 3 h; (D) bright field image, (E) the merged fluorescent image. (F) Fluorescence image at scale bar 100 µm. Deconvolution fluorescence microscopic image showing magnified image of the HeLa cells treated with composite NPs for 3 h; (H) bright field image, (I) the merged fluorescent image. (J) Fluorescence image. (K) TEM images of HeLa cells treated with the composite NPs for 3 h at 0.2 µm scale. (L) Magnified TEM image of the composite NPs of the same cell at 20 nm scale bar is showing uptake of the composite NPs inside the cell.

The uptake was further confirmed by exploiting the composite nanoparticles' luminescence property using fluorescence activated cells sorter (FACS) without addition of any conventional dye. A dose dependent study was done which revealed the maximum shift in FL3-H (Figure 4A) corresponding to the red emission compared to FL2-H and FL1-H where it was least (refer to Electronic Supplementary Information Figure S10F, S10G). For establishing the role of cytotoxic activity, 3-(4, 5-dimethylthiazolyl-2)-2, 5-diphenyltetrazolium bromide (MTT) assay was done. The results (Figure 4B) indicated that IC_{50} value of the composite NPs was at Ag concentration of 3.6 µg/mL. Also simultaneously AgNPs only was tested for cytotoxicity, which showed around 40% cell death at around 3.6 µg/mL. The amount of Au present in the composite at IC_{50} was found to be 0.068 µg/mL. The as-synthesized composite NPs were concentrated prior to use in cell viability studies. Here it may be noted that in the case of presence of gold nanoclusters along with silver nanoparticles, the activity of the composite had increased as compared to monoatomic gold nanocluster system reported earlier[47], possibly due to the synergistic effect of the bimetallic system. Here in this case, we have optimized the ratio of AgNPs and AuNCs in such a way that the cytotoxicity is retained (due to Ag) alongside with the ability to image the cells. Only 2.1:1 ratio of Ag to Au was found to satisfy both the criteria.

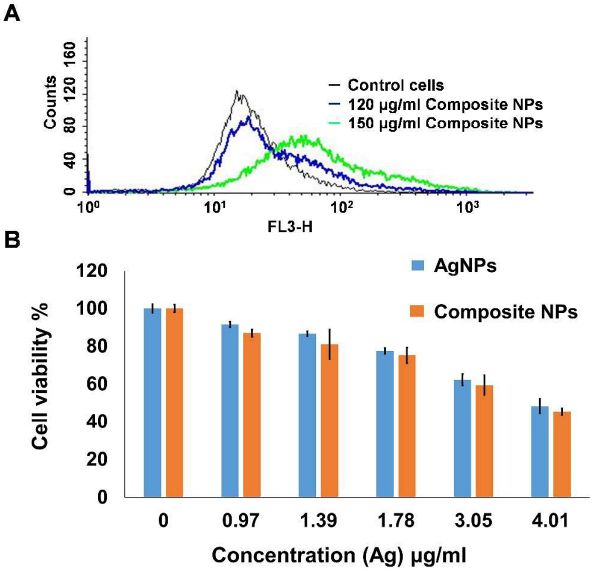

Figure 4. (A) Uptake study of the composite NPs by FACS in HeLa cells, probing the luminescence of Au NCs without using any additional dye, was carried out (5 h) after treatment with the different amounts of the composite. (B) The MTT assay of control and treated cells depicting cell viability. The values are represented as mean ± SD of three individual experiments.

The FESEM analysis of HeLa cells treated for 24 h at IC_{50} dose revealed membrane blebbing and disoriented morphology characterizing that the cells have possibly undergone programmed cell death (refer to Electronic Supplementary Information Figure S11A and S11B). Ethidium bromide/acridine orange double staining confirmed that significant percentage of cells were dead at IC_{50} when compared to the control cells (refer to Electronic Supplementary Information, Figure S12 A-12C).

In order to have a clear picture of the mechanism of cell death involved, DCFHDA staining was performed to confirm the generation of reactive oxygen species, which is the most common established mechanism of rendering a cell towards apoptosis by AgNPs. A slightly higher amount of ROS was seen to be generated in case of composite NPs compared to AgNPs only, possibly due to the presence of AuNCs along with AgNPs. Also cell cycle analysis was carried out by propidium iodide (PI) staining, which showed significant increase in sub G_0/G_1 cell population along with slight changes in other phases of cell cycle (G_0/G_1, S, and G_2/M) as shown in Figure 5A and 5B. After treatment with the composite NPs as compared to AgNPs only, which too showed increase in sub G_0-$G_{1,}$ but at a lower percentage than composite NPs. Herein, the significant increase in sub-G_0/G_1 population gives the indication of apoptosis mode of cell death (further details are available in Electronic Supplementary Information, Figure S13).

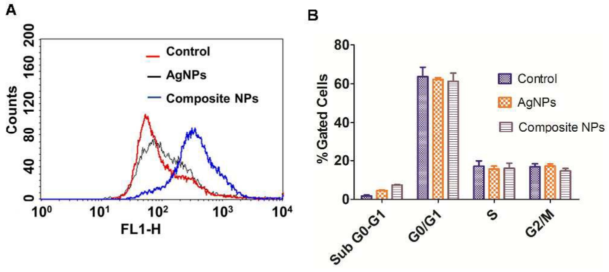

Figure 5. (A) ROS generation in case of composite NPs with respect to control and AgNPs treated cells. (B) Cell cycle analysis by FACS of the control, AgNPs treated, and the composite NPs treated cells. The data represents as mean ± SD of three individual experiments.

It was further confirmed by caspase 3 assay, which exhibited a marked increase in the percentage of apoptotic population of cells in case of composite NPs treatment as compared to AgNPs treatment only and the control cells (Figure 6A-C). Relative expression level of caspase-3 was confirmed by reverse transcription polymerase chain reaction (RT-PCR). For that the total RNA was extracted from the control untreated as well as composite NPs treated HeLa cells and was subsequently transformed into cDNA by (RT-PCR). The cDNA was used to find out the expression level of the caspase 3 by semi-quantitative polymerase chain reaction (PCR) analysis followed by the agarose gel electrophoresis. The results demonstrated that caspase 3 expression was significantly high in case of treated HeLa cells as compared to the control; while β-actin a house keeping gene, served as an endogenous control showed the similar expression level in both cases. From this, we could infer that cells started to undergo apoptosis via activation of caspases (refer to Electronic Supplementary Information Figure S14A and S14B). Hence, it is clear that the bimetallic composite NPs were effective in killing cancer cells by apoptosis with having the advantage of detection of cancer cells using photoluminescence under proper excitation.

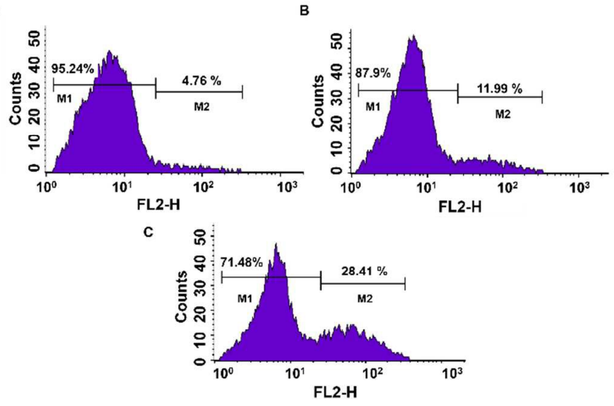

Figure 6. (A) Caspase 3 assay showing percentage of apoptosis in Control and (B) AgNPs and (C) composite NPs treated cells.

Conclusions

In brief a bimetallic NP-NC based theranostic composite NPs nanoparticles were synthesized using an easy and fast method involving minimal amount of the precursors. The prepared composite NPs were successfully internalized by HeLa cells due to the favorable size and surface charge. The uptake and subsequent morphological changes of the cell upon treatment with the composite NPs were evident. This current module enables cellular imaging due to the presence of luminescent AuNCs without use of any organic dye. Also the composite NPs when incubated with HeLa cells offered anticancer properties due to the presence of AgNPs, resulting in successful killing of cancer cells through apoptosis.

Acknowledgements

This work was supported by the Department of Biotechnology, and the Department of Electronics and Information Technology (No. 5(9)/2012-NANO (Vol. II)), Government of India. Assistance from CIF (IIT Guwahati), Center for Environment (IIT Guwahati) for Atomic Absorption spectroscopy, Dr. Sachin Mangale (GE Healthcare) for fluorescence microscopy, Rumi Khandelia, Sunil Kumar Sailapu are acknowledged.

References

1 E. K.-H. Chow and D. Ho, *Sci Transl Med*, 2013, **5**, 216rv4–216rv4.
2 R. Langer and N. A. Peppas, *AIChE J.*, 2003, **49**, 2990–3006.
3 T. Lammers, S. Aime, W. E. Hennink, G. Storm and F. Kiessling, *Acc. Chem. Res.*, 2011, **44**, 1029–1038.
4 D. C. Ferreira Soares, *Journal of Molecular Pharmaceutics & Organic Process Research*, 2014, **02**.
5 P. V. AshaRani, G. Low Kah Mun, M. P. Hande and S. Valiyaveettil, *ACS Nano*, 2009, **3**, 279–290.
6 H. Liu, F. Chen, P. Xi, B. Chen, L. Huang, J. Cheng, C. Shao, J. Wang, D. Bai and Z. Zeng, *J. Phys. Chem. C*, 2011, **115**, 18538–18544.

7 S. Li, X. Shen, L. Li, P. Yuan, Z. Guan, S. Q. Yao and Q.-H. Xu, *Langmuir*, 2014, **30**, 7623–7627.
8 K. Bhattacharyya, B. S. Goldschmidt, M. Hannink, S. Alexander and J. A. Viator, *Clin Lab Med*, 2012, **32**, 89–101.
9 U. Resch-Genger, M. Grabolle, S. Cavaliere-Jaricot, R. Nitschke and T. Nann, *Nat Meth*, 2008, **5**, 763–775.
10 L. Shang, S. Dong and G. U. Nienhaus, *Nano Today*, 2011, **6**, 401–418.
11 X. Qu, Y. Li, L. Li, Y. Wang, J. Liang and J. Liang, *Journal of Nanomaterials*, Article ID 784097, in press.
12 J. Zheng, C. Zhang and R. M. Dickson, *Phys. Rev. Lett.*, 2004, **93**, 077402.
13 J. Xie, Y. Zheng and J. Y. Ying, *J. Am. Chem. Soc.*, 2009, **131**, 888–889.
14 G. Li and R. Jin, *Acc. Chem. Res.*, 2013, **46**, 1749–1758.
15 L.-Y. Chen, C.-W. Wang, Z. Yuan and H.-T. Chang, *Anal. Chem.*, 2015, **87**, 216–229.
16 X. Huang, Y. Luo, Z. Li, B. Li, H. Zhang, L. Li, I. Majeed, P. Zou and B. Tan, *J. Phys. Chem. C*, 2011, **115**, 16753–16763.
17 R. Khandelia, S. Bhandari, U. N. Pan, S. S. Ghosh and A. Chattopadhyay, *Small*, 2015, n/a–n/a.
18 X. Le Guevel, IEEE Journal of Selected Topics in Quantum Electronics, 2014, **20**, 45–56.
19 L. Shang, R. M. Dörlich, S. Brandholt, R. Schneider, V. Trouillet, M. Bruns, D. Gerthsen and G. U. Nienhaus, *Nanoscale*, 2011, **3**, 2009–2014.
20 M. Banerjee, S. Sharma, A. Chattopadhyay and S. S. Ghosh, *Nanoscale*, 2011, **3**, 5120–5125.
21 X. Yuan, X. Dou, K. Zheng and J. Xie, *Part. Part. Syst. Charact.*, 2015, doi: 10.1002/ppsc.201400212.
22 I. Ortac, D. Simberg, Y. Yeh, J. Yang, B. Messmer, W. C. Trogler, R. Y. Tsien and S. Esener, *Nano Lett.*, 2014, **14**, 3023–3032.
23 E. González, J. Arbiol and V. F. Puntes, *Science*, 2011, **334**, 1377–1380.
24 S. Link, Z. L. Wang and M. A. El-Sayed, *J. Phys. Chem. B*, 1999, **103**, 3529–3533.
25 D. Wang and Y. Li, *Adv. Mater.*, 2011, **23**, 1044–1060.
26 P.-C. Chen, J.-Y. Ma, L.-Y. Chen, G.-L. Lin, C.-C. Shih, T.-Y. Lin and H.-T. Chang, *Nanoscale*, 2014, **6**, 3503–3507.
27 X. L. Guével, V. Trouillet, C. Spies, K. Li, T. Laaksonen, D. Auerbach, G. Jung and M. Schneider, *Nanoscale*, 2012, **4**, 7624–7631.
28 L. Dong, M. Li, S. Zhang, J. Li, G. Shen, Y. Tu, J. Zhu and J. Tao, *Small*, 2015, doi: 10.1002/smll.201403481.
29 S. Ristig, D. Kozlova, W. Meyer-Zaika and M. Epple, *J. Mater. Chem. B*, 2014, **2**, 7887–7895.
30 S. Ganta, H. Devalapally, A. Shahiwala and M. Amiji, *J Control Release*, 2008, **126**, 187–204.
31 J. Chen, J. Ding, C. Xiao, X. Zhuang and X. Chen, *Biomater. Sci.*, 2015, **3**, 988–1001.
32 T. López-León, E. L. S. Carvalho, B. Seijo, J. L. Ortega-Vinuesa and D. Bastos-González, *Journal of Colloid and Interface Science*, 2005, **283**, 344–351.
33 S. Rodrigues, M. Dionísio, C. R. López and A. Grenha, *Journal of Functional Biomaterials*, 2012, **3**, 615–641.
34 S. B. Sonone, S. P. Kokane, P. J. Shirote and N. S. Naikawade, *Arabian Journal of Chemistry,*2015.
35 J. Wang, G. Zhang, Q. Li, H. Jiang, C. Liu, C. Amatore and X. Wang, *Scientific Reports*, 2013, 3.
36 E. J. Goh, K. S. Kim, Y. R. Kim, H. S. Jung, S. Beack, W. H. Kong, G. Scarcelli, S. H. Yun and S. K. Hahn, *Biomacromolecules*, 2012, **13**, 2554–2561.
37 H. He, X. Wang, Z. Feng, T. Cheng, X. Sun, Y. Sun, Y. Xia, S. Wang, J. Wang and X. Zhang, *J. Mater. Chem. B*, 2015, **3**, 4786–4789.
38 T. X. Phuoc, *Journal of Materials Science and Nanotechnology*, 2014, **1**.
39 A. Murugadoss and A. Chattopadhyay, *Nanotechnology*, 2008, **19**, 015603.
40 P. Calvo, C. Remuñán-López, J. L. Vila-Jato and M. J. Alonso, *J. Appl. Polym. Sci.*, 1997, **63**, 125–132.
41 S. Underwood and P. Mulvaney, *Langmuir*, 1994, **10**, 3427–3430.
42 A. Ravindran, N. Chandrasekaran and A. Mukherjee, *Current Nanoscience*, 2012, **8**, 141–149.
43 T. Zhou, L. Lin, M. Rong, Y. Jiang and X. Chen, *Anal. Chem.*, 2013, **85**, 9839–9844.
44 K. R. Krishnadas, T. Udayabhaskararao, S. Choudhury, N. Goswami, S. K. Pal and T. Pradeep, *Eur. J. Inorg. Chem.*, 2014, **2014**, 908–916.
45 B. Paramanik and A. Patra, J. Mater. Chem. C, 2014, 2, 3005–3012; Negishi, Y.; Tsukuda, T. *Chem. Phys. Lett.* 2004, **383**, 161– 165.
46 T. Udayabhaskararao, Y. Sun, N. Goswami, S. K. Pal, K. Balasubramanian and T. Pradeep, Angew. Chem., 2012, **124**, 2197–2201.
47 A. K. Sahoo, S. Banerjee, S. S. Ghosh and A. Chattopadhyay, *ACS Appl. Mater. Interfaces*, 2014, **6**, 712–724
48 X. L. Guével, V. Trouillet, C. Spies, K. Li, T. Laaksonen, D. Auerbach, G. Jung and M. Schneider, *Nanoscale*, 2012, **4**, 7624–7631.
49 J. Sun, H. Wu and Y. Jin, *Nanoscale*, 2014, **6**, 5449–5457.
50 N. Zhang, Y. Si, Z. Sun, L. Chen, R. Li, Y. Qiao and H. Wang, *Anal. Chem.*, 2014, **86**, 11714–11721.
51 C.-A. J. Lin, T.-Y. Yang, C.-H. Lee, S. H. Huang, R. A. Sperling, M. Zanella, J. K. Li, J.-L. Shen, H.-H. Wang, H.-I. Yeh, W. J. Parak and W. H. Chang, *ACS Nano*, 2009, **3**, 395–401.
52 L. Qi, Z. Xu, X. Jiang, C. Hu and X. Zou, *Carbohydrate Research*, 2004, **339**, 2693–2700.
53 D. Wei, W. Sun, W. Qian, Y. Ye and X. Ma, *Carbohydrate Research*, 2009, **344**, 2375–2382.
54 Q. Yao, Z. Luo, X. Yuan, Y. Yu, C. Zhang, J. Xie and J. Y. Lee, *Sci. Rep.*, 2014, **4**.
55 G. Sahay, D. Y. Alakhova and A. V. Kabanov, *J Control Release*, 2010, **145**, 182–195.
56 D. Peer, J. M. Karp, S. Hong, O. C. Farokhzad, R. Margalit and R. Langer, *Nat Nano*, 2007, **2**, 751–760.